PSFC/JA-99-24

Matched Filtering for the Measurement of Ducted VLF Emissions

M.J. Starks[1,2] and M.C. Lee[1]

[1.] Massachusetts Institute of Technology, Cambridge, MA, 02139

[2.] Now at: Air Force Research Laboratory, Hanscom AFB, MA 01731

Abstract

The application of matched filtering to the problem of very low frequency (VLF) radio signals ducted between magnetically conjugate points on the Earth by ionospheric plasma structures has been examined theoretically and implemented in recent field experiments. With accurate knowledge of the source VLF emissions, the subionospheric component of the received waveform can be effectively removed and the characteristics of the remaining ducted signal accurately estimated. Although the technique has been shown not to produce strictly consistent estimates of the subionospheric and ducted signal amplitudes, it is able to efficiently recover the transit delays and amplitudes of ducted man-made whistler-mode emissions for reasonable values of the relevant signal to noise ratios. This is substantiated by the use of matched filtering to analyze data collected by radio receivers placed at the conjugate ends of a magnetic field line, thereby recovering the amplitudes and transit delays of ducted signals with time-resolution as small as 30 seconds. An arbitrary degree of accuracy can be obtained in these measurements through the use of bit stream extraction and comparison.

1. INTRODUCTION

The measurement of VLF signals ducted along the Earth's magnetic field has been routinely practiced since the early work of Storey [1953]. During much of the time since then, the standard instrument has been the spectrographic receiver such as that used by Carpenter [1963] to make the first observations of the plasmasphere. This single-ended technique utilizes one radio receiver capable of recording a Fourier-space representation of the received signals. This was followed by the introduction of the first correlation receiver [*Thomson*, 1975], which relies on antenna nulling to separate the subionospheric and ducted signals at a single monitoring site. The resulting signals are used to compute correlation coefficients that are integrated for 15 minutes or more to identify duct transit delays and phase shifts. This technique was later refined for use with fixed Navy transmitters emitting minimum-shift keyed (MSK) signals [*Thomson,* 1981]. Cross-correlations are performed on bit-extracted signals rather than raw waveforms by beating the signal with one of the fundamental MSK carriers. The resulting pattern can be decoded into binary digits, which are then processed by a discrete-time cross-correlator and subjected to integration.

Although the cross-correlation technique is similar to matched filtering in operation, it is not truly a matched process as described in this paper. Without accurate knowledge of the signal radiated by the Navy transmitter the subionospheric component of the received waveform cannot be efficiently removed, nor can the quality of a ducting measurement be accurately estimated. Efforts to use true matched filtering in the past [*Hamar and Tarcsai,* 1982] have been limited to natural whistler waves, and relied upon somewhat speculative models of nose whistler waveforms produced by parameter

estimation. The technique has been used primarily to identify the transit delays of individual nose whistlers in environments suffering severe multi-path effects.

There exists, then, a need to investigate the use of matched filtering for identifying ducted low-frequency transmissions in signals recorded at conjugate stations. The requirement that an accurate source image be available essentially restricts its application to man-made emissions from fixed transmitters, making the US Navy's VLF communications network an ideal signal source. This work demonstrates the utility of this technique on both theoretical and experimental grounds. We first describe its implementation in mathematical terms and then report verified measurements of ducting events obtained by using the technique on actual data from field experiments.

2. MATCHED FILTERING

Matched filtering is commonly used in the communications field as a means of detecting and identifying symbols from a known alphabet that have been transmitted over some type of channel. In doing so, a receiver makes use of a stored table of all possible symbols and compares them with the incoming signal. Whichever symbol most closely matches the transmission under the chosen figure of merit is then forwarded to the next stage of the receiver as the correct message. As an extension of this process, entire waveforms consisting of many symbols may be substituted for individual characters and the presence or absence of a given message within a received signal established on statistical grounds, as well as the relative amplitude and time delay with which it appears.

In the case of emissions from fixed VLF transmitters, signals recorded at the magnetic conjugate point can be processed by matched filter to obtain the subionospheric

transit time and amplitude. When it is not possible to control the content of the MSK signal from a particular transmitter, a second radio receiver can be placed in proximity to the emitting antenna to record a nearly uncontaminated source image. This image is then used as the reference signal for the matched filter and, in conjunction with the amplitude and phase information thus obtained, allows nearly complete removal of the subionospheric component from the conjugate data. Reapplying the matched filter to the resulting data then reveals any ducted emissions and provides their corresponding amplitudes and transit delays.

For example, consider the narrowband MSK transmitter time-function to be given by *s(t)*. A VLF receiver located in close proximity to this transmitter records the signal $r_1(t)$, where

$$r_1(t) = s(t) + m(t) \tag{1}$$

and *m(t)* is a noise term representing any contaminating multipath, interference, equipment or other additive noise effects. Emissions from the VLF source propagate primarily in the Earth-ionosphere waveguide, but some energy can be converted into the whistler mode and coupled into field-aligned plasma ducts. In the presence of such ducting, a VLF receiver located near the transmitter's magnetic conjugate location will record the signal $r_2(t)$, where

$$r_2(t) = as(t - t_0) + bs(t - t_1) + n(t) \tag{2}$$

and a and t_0 are the subionospheric signal's amplitude and transit delay, b and t_1 are the ducted signal's amplitude and transit delay and $n(t)$ is a noise term similar to that found in (1).

The simplest implementation of a matched filter is the so-called correlation receiver, the principles of which are also used by Thomson [1975, 1981]. The signal $r_2(t)$ is cross-correlated with the source image (provided here by $r_1(t)$) to produce

$$\begin{aligned} R_{r1r2}(t) &= \frac{1}{T}\int_0^T r_1(t-\tau)r_2(\tau)d\tau \\ &= \frac{1}{T}\int_0^T [s(t-\tau)+m(t-\tau)][as(\tau-t_0)+bs(\tau-t_1)+n(\tau)]d\tau \\ &= \frac{1}{T}\int_0^T as(t-\tau)s(\tau-t_0)+bs(t-\tau)s(\tau-t_1)+m(t-\tau)n(\tau)d\tau \\ &= aR_{ss}(t-t_0)+bR_{ss}(t-t_1) \end{aligned} \tag{3}$$

where $R_{ss}(t)$ is the autocorrelation function of the transmitted waveform $s(t)$. We have assumed that the VLF transmitter signal $s(t)$ is uncorrelated with the noise processes $m(t)$ and $n(t)$ (typically a very good approximation), and that the noise processes are not correlated with one another (which may not be true in practice). Note that a long data period T is required to eliminate cross-coupling between terms that are uncorrelated as $T\rightarrow\infty$ and in practice there will be some contamination remaining due to these cross terms. Since the magnitude of the subionospheric signal is much greater than that of the ducted signal, we may take a to be much greater than b. By identifying the largest peak of $R_{r1r2}(t)$, we recover the subionospheric signal's transit time t_0 and estimate its amplitude to be

$$\hat{a} = \frac{R_{r1r2}(t_0)}{R_{r1r1}(0)} = a\frac{R_{ss}(0)}{R_{r1r1}(0)} + b\frac{R_{ss}(t_0 - t_1)}{R_{r1r1}(0)} \approx a + b\frac{R_{ss}(t_0 - t_1)}{R_{ss}(0)} \tag{4}$$

where $R_{r1r1}(t)$ is the autocorrelation of the source image $r_1(t)$. We have assumed that the signal-to-noise ratio (SNR) of $r_1(t)$ is very high such that the contribution of $m(t)$ to $R_{r1r1}(t)$ is minimal. Note that $R_{ss}(t_0–t_1)$ is typically much less than $R_{ss}(0)$.

We may now remove the subionospheric contribution from the conjugate data using the estimates of t_0 and a provided by the matched filter.

$$\begin{aligned} r_2'(t) &= r_2(t + t_0) - \hat{a} r_1(t) \\ &= \left[-b\frac{R_{ss}(t_0 - t_1)}{R_{ss}(0)} \right] [s(t) + m(t)] + bs(t + t_0 - t_1) + n(t + t_0) - am(t) \\ &= cs(t) + bs(t + t_0 - t_1) + (c - a)m(t) + n(t + t_0) \end{aligned} \tag{5}$$

where $c = -b\,R_{ss}(t_0 - t_1)/R_{ss}(0)$.

Applying the filter again, we have

$$\begin{aligned} R_{r1r2'}(t) &= \frac{1}{T}\int_0^T r_1(t - t')r_2'(t')dt \\ &= \frac{1}{T}\int_0^T [s(t - t') + m(t - t')][cs(t') + bs(t' + t_0 - t_1) + (c - a)m(t') + n(t' + t_0)]dt \\ &\cong \frac{1}{T}\int_0^T [cs(t - t')s(t') + bs(t - t')s(t' + t_0 - t_1) + (c - a)m(t - t')m(t')]dt \\ &= cR_{ss}(t) + bR_{ss}(t + t_0 - t_1) + (c - a)R_{mm}(t) \end{aligned} \tag{6}$$

Since $c << b$ and the source image SNR is large so that $|bR_{ss}(0)| >> |(c\text{-}a)R_{mm}(t_1\text{-}t_0)|$, we may immediately estimate the ducted signal's transit delay t_1 and amplitude from

$$\hat{b} = \frac{R_{r1r2'}(t_1 - t_0)}{R_{r1r1}(0)} \approx b\left[1 - \frac{R_{ss}(t_1 - t_0)R_{ss}(t_0 - t_1)}{R_{ss}{}^2(0)}\right] \tag{7}$$

In practice, $t_1 >> t_0$ and the quantity in brackets is close to one.

When applied in actual field use, the process described above must operate on sampled data segments of finite length. The results shown here for the continuous-time case hold in the finite-length discrete-time case as long as unbiased estimates of the correlation functions are computed. In addition, the lengths of the data segments are critical to the quality of the results. The subionospheric signal is well-known to be extremely phase stable, so that even very long data segments can be successfully integrated without difficulty. By contrast, the ducted signal exhibits phase variations of up to several hundred milliHertz and long cross-correlations will typically sum to zero [*Thomson,* 1981]. Data segments of appropriate length must therefore be used when applying the matched filter for the second time; lengths of one second or less are recommended. Note that with suitable modification the filter can detect ducted emissions with transit delays much longer than the data segment length.

3. ERROR ANALYSIS

The process of matched filtering is easily understood in cases of very long continuous-time signals such as those used above to illustrate the technique. In practice, the available data will be discrete, band-limited and finite in length. While band-limiting simply leads to additional clutter in the autocorrelation domain, the behavior of the

detector for finite-length sampled sequences is less obvious. This is briefly examined here.

Consider sampled waveforms from each of the conjugate receiving sites. Assume that $r_1[k]$ is the source image recording, composed of the actual transmission $s[k]$ and contaminating zero-mean additive white Gaussian noise (AWGN) $m[k]$ with variance σ^2_m. $r_2[k]$ is the received signal, composed of a subionospheric component with amplitude a and delay of t_0 samples, a ducted component with amplitude b and delay of t_1 samples, and zero-mean AWGN $n[k]$ with variance σ^2_n.

$$\begin{aligned} r_1[k] &= s[k] + m[k] \\ r_2[k] &= as[k - t_0] + bs[k - t_1] + n[k] \end{aligned} \tag{8}$$

We assume that our sequences are M_0 points long. To carry out the matched filtering, we compute cross-correlation functions as follows

$$R_{xy}[k] = \frac{1}{2M+1} \sum_{l=-M}^{l=M} x[l]y[l+k] \tag{9}$$

where $M << M_0$. As outlined in the section above, we form the cross-correlation sequence $R_{r1r2}[k]$:

$$\begin{aligned} R_{r1r2}[k] = \frac{1}{2M+1} \sum_{l=-M}^{l=M} & as[l]s[l - t_0 + k] + bs[l]s[l - t_1 + k] + s[l]n[l+k] + \\ & am[l]s[l - t_0 + k] + bm[l]s[l - t_1 + k] + m[l]n[l+k] \end{aligned} \tag{10}$$

and evaluate it at $k = t_0$. We assume that $t_0 << t_1$ and $a >> b$ so that the value of t_0 will be obvious from inspecting $R_{r1r2}[k]$, and take it to be a known parameter. The estimate of the amplitude a is then given by

$$\hat{a} \equiv \frac{R_{r1r2}[t_0]}{R_{r1r1}[0]} \tag{11}$$

where

$$R_{r1r1}[0] = \frac{1}{2M+1}\sum_{l=-M}^{M} s^2[l] + 2s[l]m[l] + m^2[l] \tag{12}$$

We may decompose the estimate $\hat{a}$ into constant components (denoted with an overbar) and random components (prefixed with a D).

$$\hat{a} = \frac{\overline{R}_{r1r2}[t_0] + \Delta R_{r1r2}[t_0]}{\overline{R}_{r1r1}[0] + \Delta R_{r1r1}[0]} = \frac{\overline{R}_{r1r2}[t_0]}{\overline{R}_{r1r1}[0]}\left[1 + \frac{\Delta R_{r1r2}[t_0]}{\overline{R}_{r1r2}[t_0]}\right]\left[1 + \frac{\Delta R_{r1r1}[0]}{\overline{R}_{r1r1}[0]}\right]^{-1} \tag{13}$$

(13) can be linearized by applying the binomial theorem and discarding higher order terms as long as the following condition is met

$$\overline{R}^2_{r1r1}[0] >> \Delta R^2_{r1r1}[0] \tag{14}$$

We will analyze this condition in more detail later, but for now we simply assume that M and the source image SNR are sufficiently large – conditions which cause (14) to be satisfied.

The linearized estimate is then given by

$$\hat{a} \cong \frac{\overline{R}_{r1r2}[t_0]}{\overline{R}_{r1r1}[0]}\left[1+\frac{\Delta R_{r1r2}[t_0]}{\overline{R}_{r1r2}[t_0]}-\frac{\Delta R_{r1r1}[0]}{\overline{R}_{r1r1}[0]}\right] \tag{15}$$

and we can compute the mean of the estimate simply.

$$\begin{aligned}\overline{\hat{a}} &= \frac{\overline{R}_{r1r2}[t_0]}{\overline{R}_{r1r1}[0]} = \frac{\sum_{l=-M}^{M} as^2[l]+\sum_{l=-M}^{M} bs[l]s[l-t_1+t_0]}{\sum_{l=-M}^{M} s^2[l]+(2M+1)s_m^2} \\ &= \frac{a\left[1+\frac{b}{a}\frac{R_{ss}[t_0-t_1]}{R_{ss}[0]}\right]}{1+\frac{s_m^2}{R_{ss}[0]}} \cong \frac{a}{1+(SNR_{src})^{-1}}\end{aligned} \tag{16}$$

where we have defined the signal-to-noise ratio of the source image $r_1[k]$ in the usual way.

Figure 1 demonstrates clearly that the estimate of the subionospheric amplitude is biased for all lengths M and is therefore not consistent. However, for respectable values of SNR we can successfully remove most of the subionospheric signal.

The variance of $\hat{a}$ is given by

$$\mathrm{var}(\hat{a}) = \bar{\hat{a}}^2 \left[\frac{\mathrm{var}(\Delta R_{r1r2}[t_0])}{\bar{R}^2_{r1r2}[t_0]} + \frac{\mathrm{var}(\Delta R_{r1r1}[0])}{\bar{R}^2_{r1r1}[0]} - \frac{2\,\mathrm{cov}(\Delta R_{r1r2}[t_0], \Delta R_{r1r1}[0])}{\bar{R}_{r1r2}[t_0]\bar{R}_{r1r1}[0]} \right] \tag{17}$$

If we assume that M is large, $R_{ss}(t_1\text{-}t_0) \gg 0$ and $b^2/a^2 \ll 1$, a significant amount of algebra reduces (17) to

$$\mathrm{var}(\hat{a}) \approx \frac{a^2}{2M} \left[\frac{1}{SNR_{src}} + \frac{1}{SNR_{sub}} \right] \tag{18}$$

where a is less than one and we have defined the SNR of the subionospheric signal as

$$SNR_{sub} = \frac{a^2 \left(\frac{1}{2M+1} \right) \sum_{l=-M}^{M} s^2[l]}{s_n^2} \tag{19}$$

A normalized version of (18) is plotted in Figure 2. Note that both the subionospheric and source image SNRs determine the variance of the estimate, and that long sequences (such as those found below in Section 5) lead to very small variances.

Following a similar line of reasoning, we may define the signal $r'_2[k]$ as the received signal after removal of the subionospheric signal using the estimate $\hat{a}$.

$$r'_2[k] = (a - \hat{a})s[k - t_0] + bs[k - t_1] + n[k] - \hat{a}m[k - t_0] \tag{20}$$

A similar analysis as above shows that the mean of the ducted signal amplitude estimate is given by

$$\overline{\hat{b}} = \frac{\sum_{l=-M}^{M} bs^2[l] + \sum_{l=-M}^{M} (a-\hat{a})s[l]s[l-t_0+t_1] - \sum_{l=-M}^{M} \hat{a}m[l]m[l-t_0]}{\sum_{l=-M}^{M} s^2[l] + (2M+1)s_m^2}$$
$$= \frac{b\left[1 + \frac{a-\hat{a}}{b}\frac{R_{ss}[t_1-t_0]}{R_{ss}[0]}\right] - \hat{a}\frac{R_{mm}[t_1-t_0]}{R_{ss}[0]}}{1 + \frac{s_m^2}{R_{ss}[0]}} \cong \frac{b}{1+(SNR_{src})^{-1}} \tag{21}$$

which is similar in form to the mean of the estimate of $\hat{a}$ given in (16). The variance of the estimate takes a form like that in (18).

We now examine the limits of the linearization technique used to produce (15). The condition given in (14) can be expanded into the form

$$\left[\sum_{l=-M}^{M}\left(s^2[l] + s_m^2\right)\right]^2 >> s_m^2 \sum_{l=-M}^{M}\left(s^2[l] + 2s_m^2\right) \tag{22}$$

which readily yields

$$(2M+1)[1+SNR_{src}]^2 >> 2 + SNR_{src} \tag{23}$$

Hence the linearization is applicable for all values of SNR as long as the sequence length is significant.

This analysis demonstrates that the quality of the source image is of paramount importance in the accurate removal of the subionospheric signal from conjugate data. Under the assumptions made here, incomplete removal of this signal does not affect the detection of the ducted signal. This is because the ideal cross-correlation of even finite

sequences of an MSK signal can be shown to go to zero for time offsets larger than two bit intervals. Any remaining subionospheric component then drops out of the analysis. In practice, band-limiting of the MSK signal causes energy to spread far from the origin in the auto-correlation domain and the incomplete removal of the subionospheric signal becomes important.

Simulations of typical MSK signals subjected to band- and time-limiting similar to that found in the remainder of this work do not have ideal cross-correlations that fall to zero for time offsets larger than two bit periods. Instead, the shifted cross-correlation terms in (16) and (21) tend to contribute a small amount to the mean values of the estimates. This contribution increases with reduced sampling frequencies, primarily as a result of the implicit band-limiting taking place. In particular, simulated 9.5 kHz MSK signals of unit amplitude that are sampled at 38 ksamples/sec (parameters representative of demodulated signals found in Section 5) show that

$$\frac{1}{2M+1}\sum_{l=-M}^{M} s[l]s[l-t_0+t_1] \sim 0.1\cdot\left[\frac{1}{2M+1}\sum_{l=-M}^{M} s^2[l]\right] \tag{24}$$

If we assume that the source image is perfect, *i.e.* $s^2_m = 0$, the amplitude estimate becomes

$$\hat{a} = a + 0.1b \tag{25}$$

This error is not as severe as it might seem because the magnitude of *b* is typically only 2% of that of *a*. Continuing in this fashion, we find the error introduced into the ducted amplitudes is

$$\hat{b} = b(1-0.01) = 0.99b \tag{26}$$

Although it is difficult or impossible to consider all of the significant sources of error in this estimation problem simultaneously, when taken individually they all lead to almost insignificant errors in the final estimates. From this we can be somewhat reassured that taken together they will result in tolerable deviations from the ideal.

4. BIT EXTRACTION

A significant advantage of applying true matched filtering to detecting ducted whistlers is the ability to use bit extraction to attach accurate confidence measures to each detection. Bit extraction has been used with single-ended correlation receivers in the past, but only as a pre-processing step to prepare the data for a discrete integration. With the recovery of transit delays and amplitudes by matched filtering, however, we are free to reserve bit extraction as a means of verifying our measurements. Extraction is performed by multiplying an MSK waveform by one of the two carrier sinusoids, removing the high-frequency components, and examining the baseband results.

As an example, consider the MSK signal described by *s(t)*

$$s(t) = w(t)z(t)\cos(w_1 t) + w(t)[1-z(t)]\cos(w_2 t) \tag{27}$$

where ω_1 and ω_2 are the two MSK carrier frequencies ($\omega_1 < \omega_2$), *z(t)* is the information function taking the value of 0 or 1 over a specified bit interval, and *w(t)* is the modulation function taking the value of +1 or −1 over the bit interval in order to satisfy the continuous phase requirements of MSK modulation.

Multiply the MSK waveform by a sinusoid at the lower carrier frequency ω_1, which includes an additional phase term resulting from our inability to precisely match phase with the received signal, and filter out the high frequency image.

$$s'(t) = w(t)z(t)\cos f + w(t)[1 - z(t)]\cos[(w_2 - w_1)t + f] \tag{28}$$

The filtered signal *s'(t)* is made up of a constant component and an oscillating component. When *z(t) = 1* (a one is being transmitted), the oscillating component is eliminated and *s'(t) = w(t)cos f = ±cos f*. When *z(t) = 0* (a zero is being transmitted), the constant component is zero and only the background oscillations are present. Hence one can observe the function *s'(t)* and infer the bit sequence *z(t)* from the presence or absence of oscillation at the frequency corresponding to the bandwidth of the MSK signal. An example of this is shown in Figure 3, where individual bit periods have been marked and threshold detection of amplitude is used to distinguish the bits. This simple correlation receiver is optimal for frequency-shift keyed (FSK) transmissions, which are true orthogonal multipulse, and adequate for MSK transmissions, which are not. The Viterbi algorithm [*Viterbi*, 1967] would provide superior performance in the MSK case at the cost of added complexity.

One problem that is not addressed in the foregoing is the effect of the unknown phase f. As shown there, this phase determines the amplitude of the zero-frequency bit intervals corresponding to ones in the demodulated signal. For $\cos \phi \approx 1$, this amplitude matches that of the background oscillations and the simple threshold detection alluded to above and in Figure 3 will fail. The straightforward solution to this difficulty is to phase-lock the demodulating sinusoid to the received signal, but this is not in fact required. By computing the mean of the demodulated signal within each bit period and observing the variance of those means, it is possible to coarsely estimate the value of $\cos \phi$. For $\cos \phi \approx 1$, this variance will be large, as the means of the intervals corresponding to zero bits (oscillations) equal zero and those of intervals corresponding to one bits (constant) are some positive value. For $\cos \phi \approx 0$, the variance is small as both cases have zero mean over a bit interval. One may then choose to threshold-detect the bit-interval mean function in the former case, the raw demodulated waveform in the latter case, and either of these for the remaining cases. This approach is used in this work, and tests using simulated MSK signals in noise have shown it achieves decoded bit error rates at least as low as 10^{-2} even in data of extremely poor SNR. Although not outstanding from a communications reliability standpoint, this figure is more than adequate for the verification of ducted signal detections.

Bit extraction as described here can be applied to the source image to provide a reference bit stream. This reference can be used with bit extraction to verify the correct value of the subionospheric propagation delay t_0 from the conjugate data, as well as the validity of a ducted signal detection once the subionospheric signal has been removed. To this end, some figure of merit must be defined to represent the quality of a given

measurement. One choice is to examine a data segment and determine the longest sequence of consecutive bits which match the reference. The probability of a sequence of n such bits randomly occurring is 2^{-n} if it is assumed that bits are equiprobable. This metric is very conservative in the presence of random single errors. Another possibility is to compute the bit error rate of a given data segment by counting the number of single bit errors it contains when compared to the reference segment. A data block of length m containing k errors has a bit error rate of k/m. A completely random segment can be expected to have a bit error rate of about 0.5. This metric is tolerant of infrequent burst errors. In practice, some combination of these performance measures is appropriate and proves quite conservative. For instance, an equal weighting of each produces the following measure of confidence, where a value of one is an error-free segment and a value of zero is an abysmal reproduction.

$$conf = \frac{1}{2}\left[\left(1-2^{-n}\right)+\left(1-\frac{k}{m}\right)\right] \tag{29}$$

When searching for ducted signals using matched filtering, a successful detection of ducting requires correct estimation of the subionospheric component of the conjugate data. Hence when computing confidence values for a ducted signal it is prudent to assign a final confidence score to the ducted detection by multiplying the scores of the recovered ducted bit sequence and the subionospheric bit sequence.

The value of matched filtering coupled with bit extraction is manifest, insofar as it allows the detection of ducted VLF signals to be verified to arbitrary precision.

5. FIELD TESTING

Field experiments were carried out during the summer of 1997 to test the practical application of the matched filtering technique. MIT Broadband VLF Receivers were deployed at both ends of the L = 1.35 field line originating near the US Navy's 28.5 kHz NAU MSK VLF transmitter located near Aguada, Puerto Rico. The source image was recorded by a receiver located at the NAIC Arecibo Observatory, using a 57cm square loop antenna. The conjugate record was obtained from the coast of south-central Argentina, near Porto Madryn, using a 6m-tall equilateral triangular loop antenna. Both experimental sites used filter/demodulator units to isolate a 12 kHz band around 28.5 kHz and demodulate it to baseband. Samples were taken at 38 ksamples/second for 10 out of every 15 minutes. The remaining period was used for error-checking and archiving of data. Data were taken every night from 2100 to 0400 LT (0100 to 0800 UT) during most of the period from July 22 to July 31, 1997. No field processing of the acquired signals was carried out during the experiment beyond simple tests to verify correct equipment operation.

Following the experiment, the data archive was examined at MIT. A 1.5-hour sampling grid was applied to the entire archive, and three five-second data streams analyzed from a ten-minute window at each sample point. The grid points are shown in Figure 4. A total of 81 data segments were extracted from each of the conjugate station archives, narrowly filtered around the NAU MSK center frequency, corrected for demodulator local oscillator variances and processed by matched filter. Bit extraction was used to verify every identification of the subionospheric signal in the conjugate data and

those with confidence scores below 95% were discarded. Ducted signal candidates were examined by bit extraction as well. Based on a histogram of the resulting confidence scores (shown in Figure 5), ducted events with final confidence scores above 96% were considered verified. Nine such events were discovered during the preliminary survey, and are marked as verified on the plot of Figure 4.

The nine verified ducting events typically exhibited duct transit delays between 0.3 and 0.8 second. Six of the nine are included in time periods initially selected for focused analysis at time resolutions as small as 30 seconds. The results of this analysis are detailed in a forthcoming publication.

6. CONCLUSIONS

The matched filter technique allows efficient detection of ducted VLF emissions from fixed transmitters by combining an uncontaminated source image with data from a conjugate receiving site. By applying matched filtering with extracted bit stream comparisons, it is possible to verify detected ducting events to an arbitrary degree of certainty. Field experiments carried out along the L = 1.35 magnetic field line have demonstrated conclusively that the technique can be utilized in the study of conjugately-ducted man-made VLF signals at short time resolutions.

ACKNOWLEDGEMENTS

This work was supported by the Air Force Office of Scientific Research through grant F49620-98-1-0389 to the Massachusetts Institute of Technology (MIT). Support for M.J. Starks was provided primarily by a US Air Force Senior Knight appointment, and

partially by a National Science Foundation Graduate Research Fellowship and an Air Force Office of Scientific Research Graduate Summer Research fellowship at the Air Force Research Laboratory. Travel funds for the conjugate-point experiments were partially provided by the National Science Foundation through grant ATM-9804324. Prof. Jeff Shapiro provided advice for completing the analysis in Section 3. Dr. Bill Burke of the Air Force Research Laboratory provided helpful comments on early versions of this paper. M.C. Lee would like to thank his students, P. Jastrzebski, K.R. O'Donnell and S.L. Meredith for assistance in recording VLF data in Argentina.

REFERENCES

Carpenter D.L., Whistler evidence of a 'knee' in the magnetospheric ionization density profile, *J. Geophys. Res., 68,* 1675, 1963.

Hamar, D., G. Tarcsai, High resolution frequency-time analysis using digital matched filtering, part I, theory and simulation study, *Ann. Geophys., 38,* 119, 1982.

Storey, L.R.O., An investigation of whistling atmospherics, *Phil. Trans. R. Soc. Lond., 246,* 113, 1953.

Thomson, N.R., Whistler mode signals: group delay by cross-correlation, *Geophys Res. Lett, 2,* 451, 1975.

Thomson, N.R., Whistler mode signals: spectrographic group delays, *J. Geophys. Res, 86,* 4795, 1981.

Viterbi, A.J., Error bounds for convolutional codes and an asymptotically optimum decoding algorithm, *IEEE Trans. Inform. Theory, IT-13,* 260, 1967.

FIGURE CAPTIONS

Figure 1: Normalized mean of the amplitude estimate in (16) plotted versus the SNR of the source image.

Figure 2: Normalized variance of the amplitude estimate as given by (18), plotted versus the source (or subionospheric) SNR.

Figure 3: Example of bit extraction demonstrating the demodulated waveform and the actual and decoded sequence (bit periods are indicated by vertical lines). Simple amplitude thresholds are used to distinguish the bits, and are shown as horizontal lines. The unknown phase f has been set to zero.

Figure 4: Results of the initial data survey. All examined data points are shown and classified. Verified ducting events are those with confidence scores exceeding 96%.

Figure 5: Histogram of confidence scores computed for the 42 potential ducting events identified during the preliminary data survey. Events with scores above 96% are considered verified.

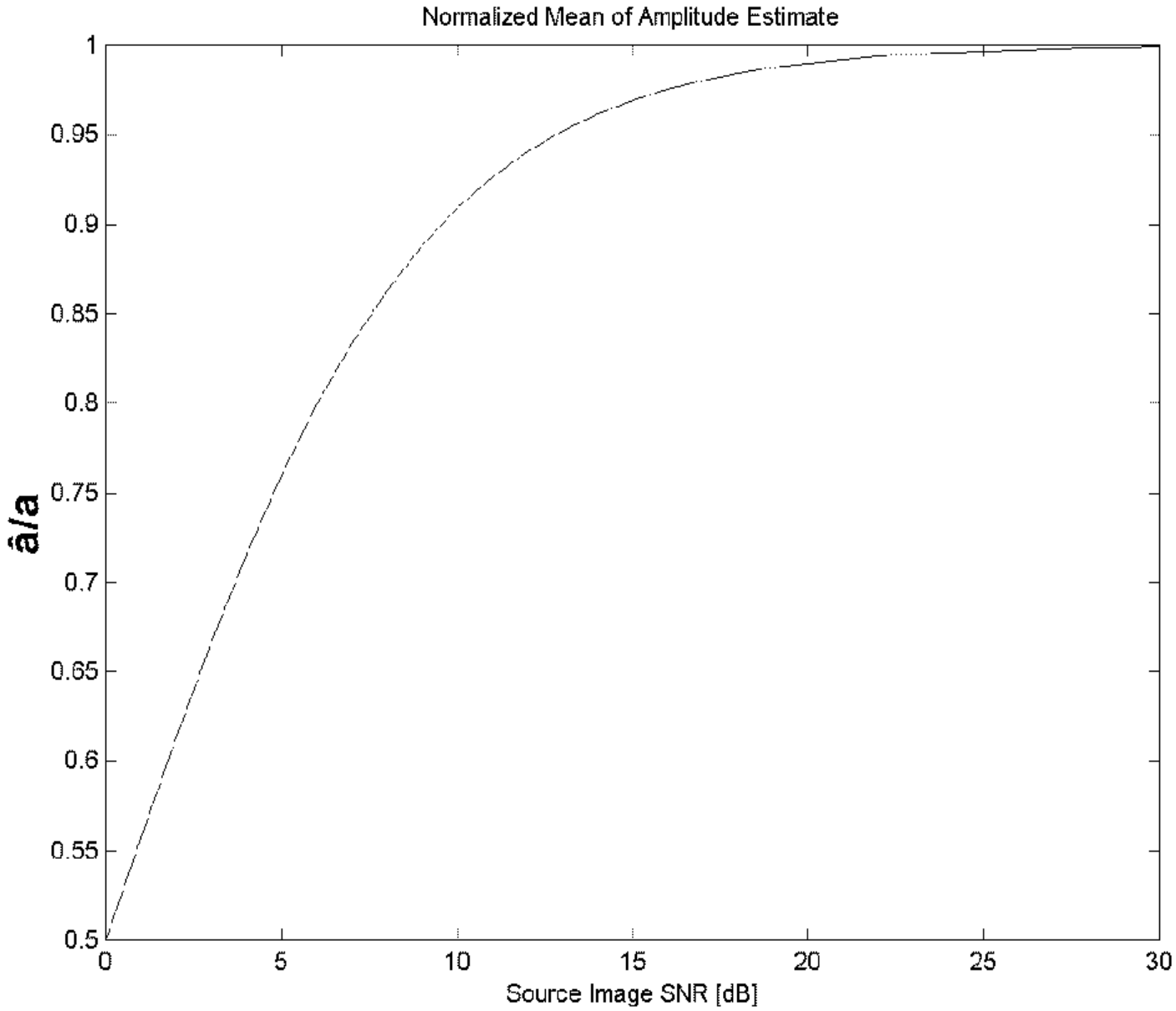
Normalized Mean of Amplitude Estimate
â/a
1
0.95
0.9
0.85
0.8
0.75
0.7
0.65
0.6
0.55
0.5
0
5
10
15
20
25
30
Source Image SNR [dB]

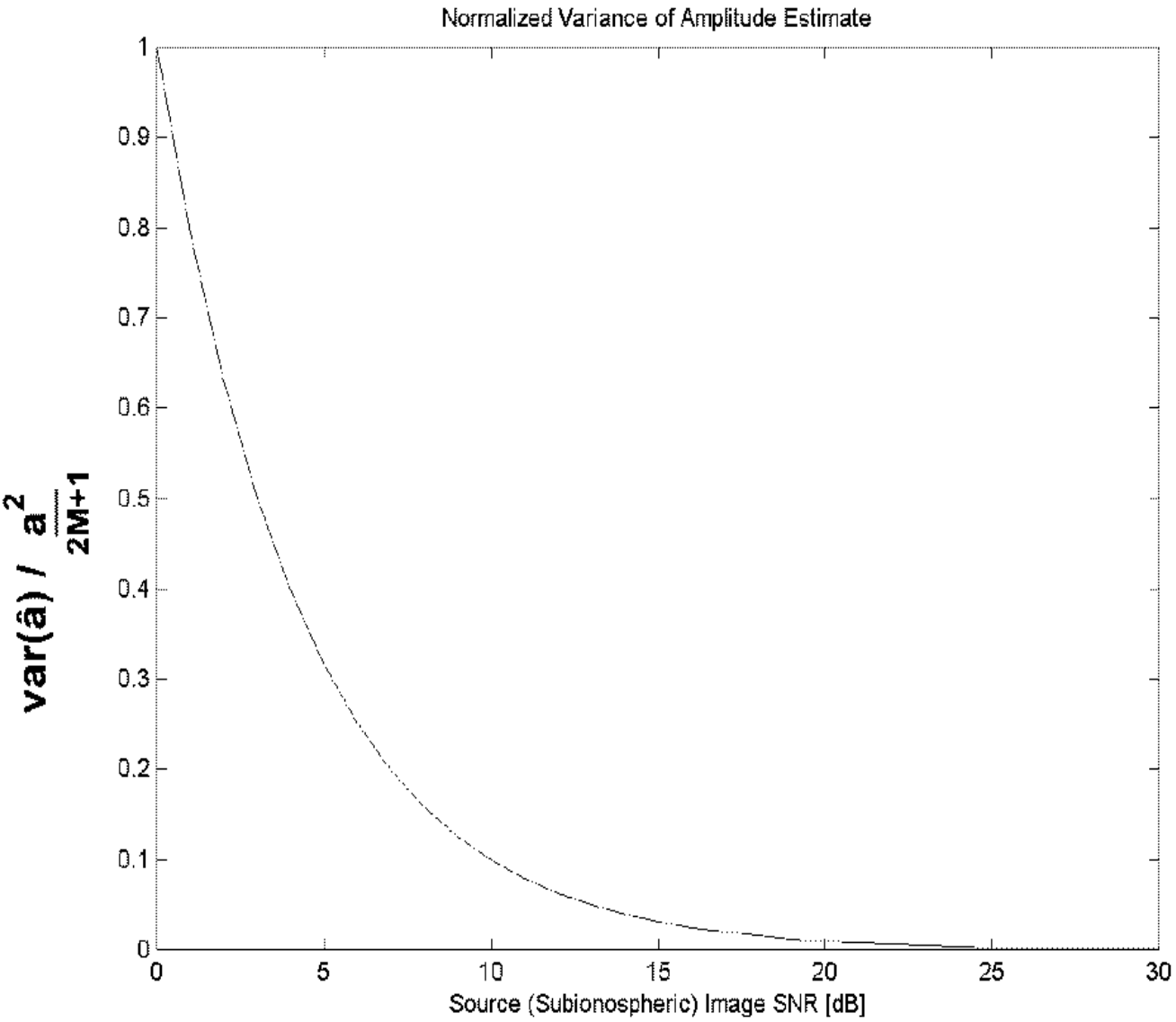
Normalized Variance of Amplitude Estimate
var(â) / a²/(2M+1)
1
0.9
0.8
0.7
0.6
0.5
0.4
0.3
0.2
0.1
0
0
5
10
15
20
25
30
Source (Subionospheric) Image SNR [dB]

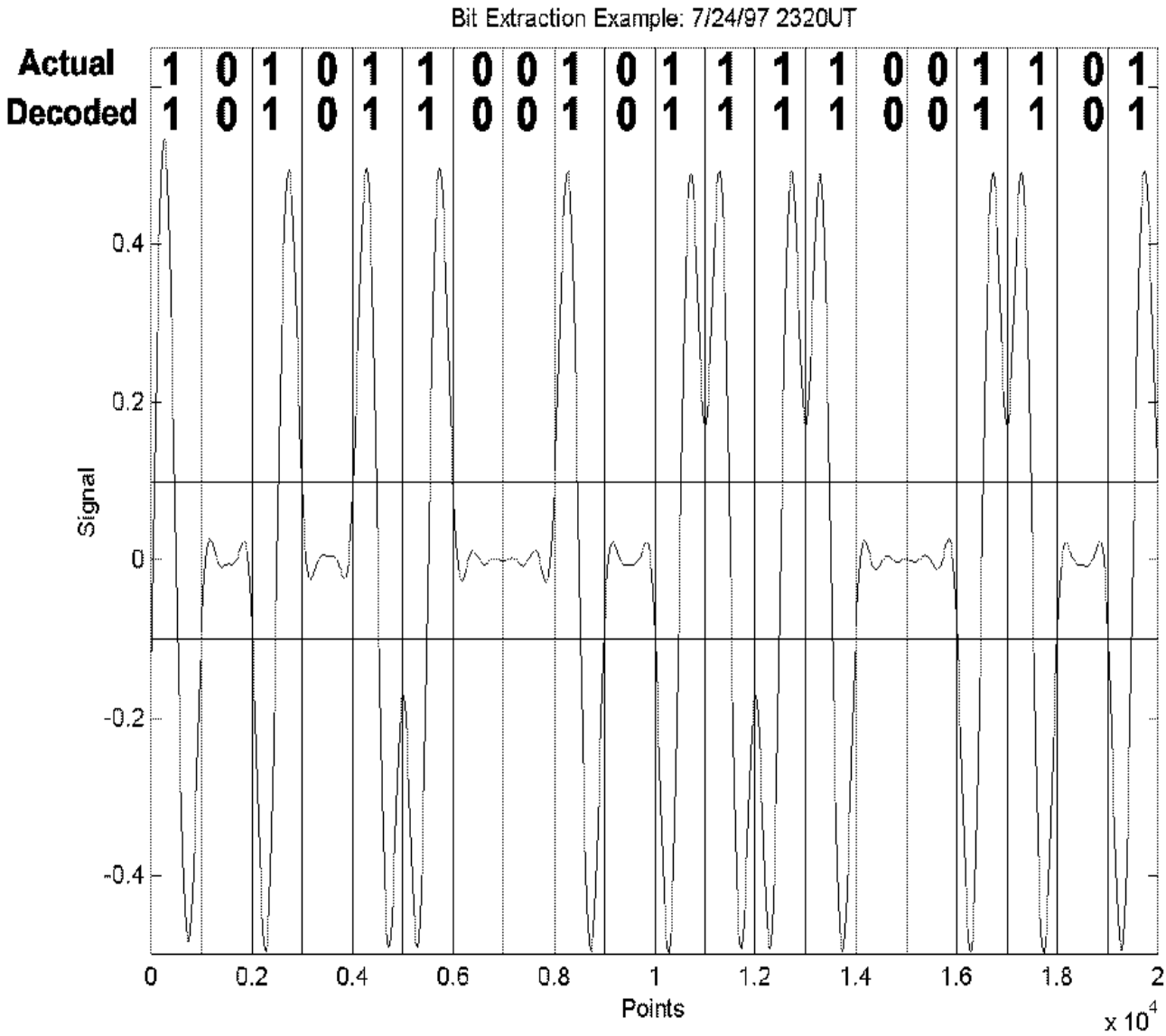
Bit Extraction Example: 7/24/97 2320UT
Actual 1 0 1 0 1 1 0 0 1 0 1 1 1 1 0 0 1 1 0 1
Decoded 1 0 1 0 1 1 0 0 1 0 1 1 1 1 0 0 1 1 0 1
Signal
0.4
0.2
0
-0.2
-0.4
0
0.2
0.4
0.6
0.8
1
1.2
1.4
1.6
1.8
2
Points
x 10^4

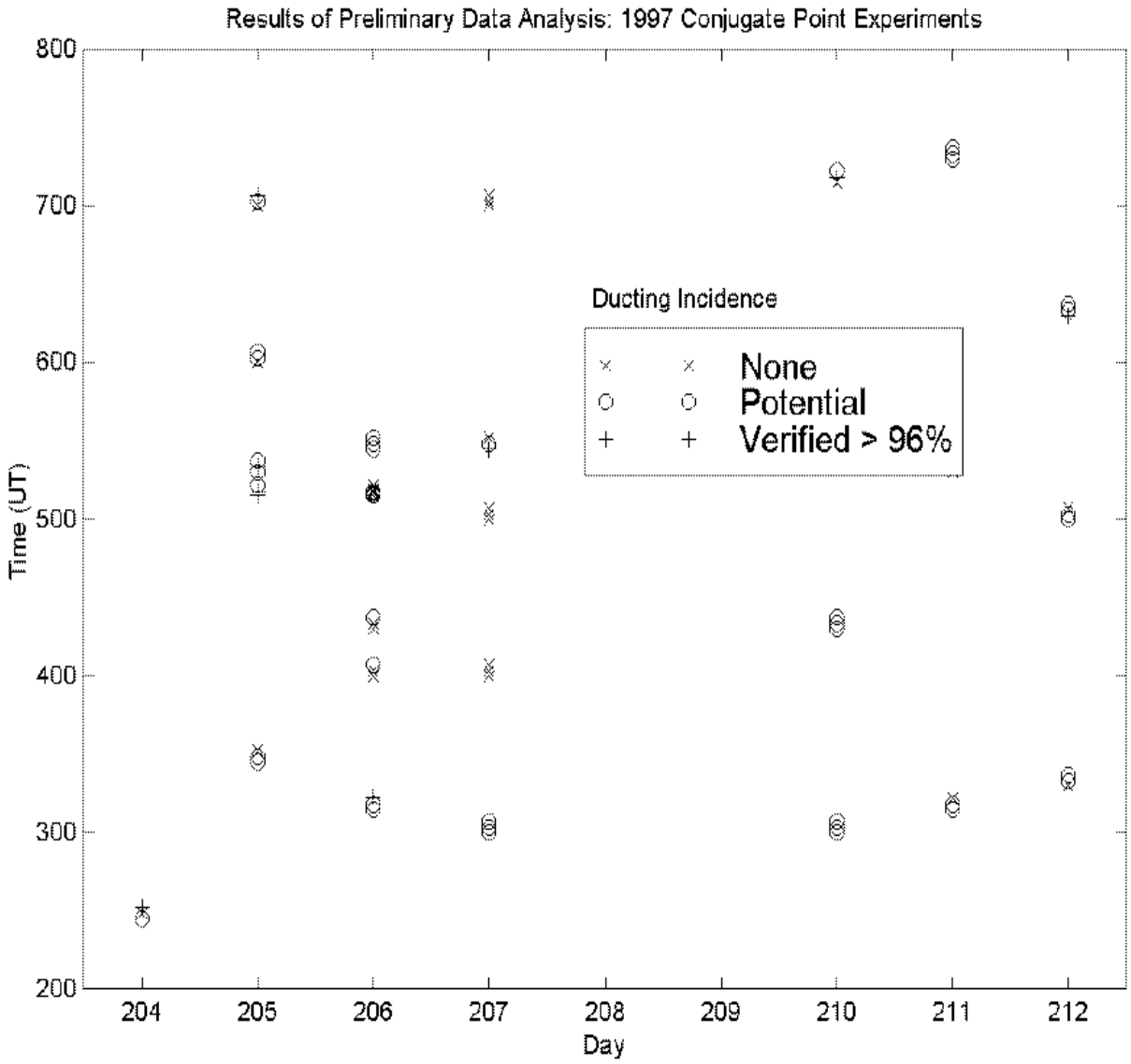
Results of Preliminary Data Analysis: 1997 Conjugate Point Experiments
Ducting Incidence
None
Potential
Verified > 96%
Time (UT)
Day
800
700
600
500
400
300
200
204
205
206
207
208
209
210
211
212

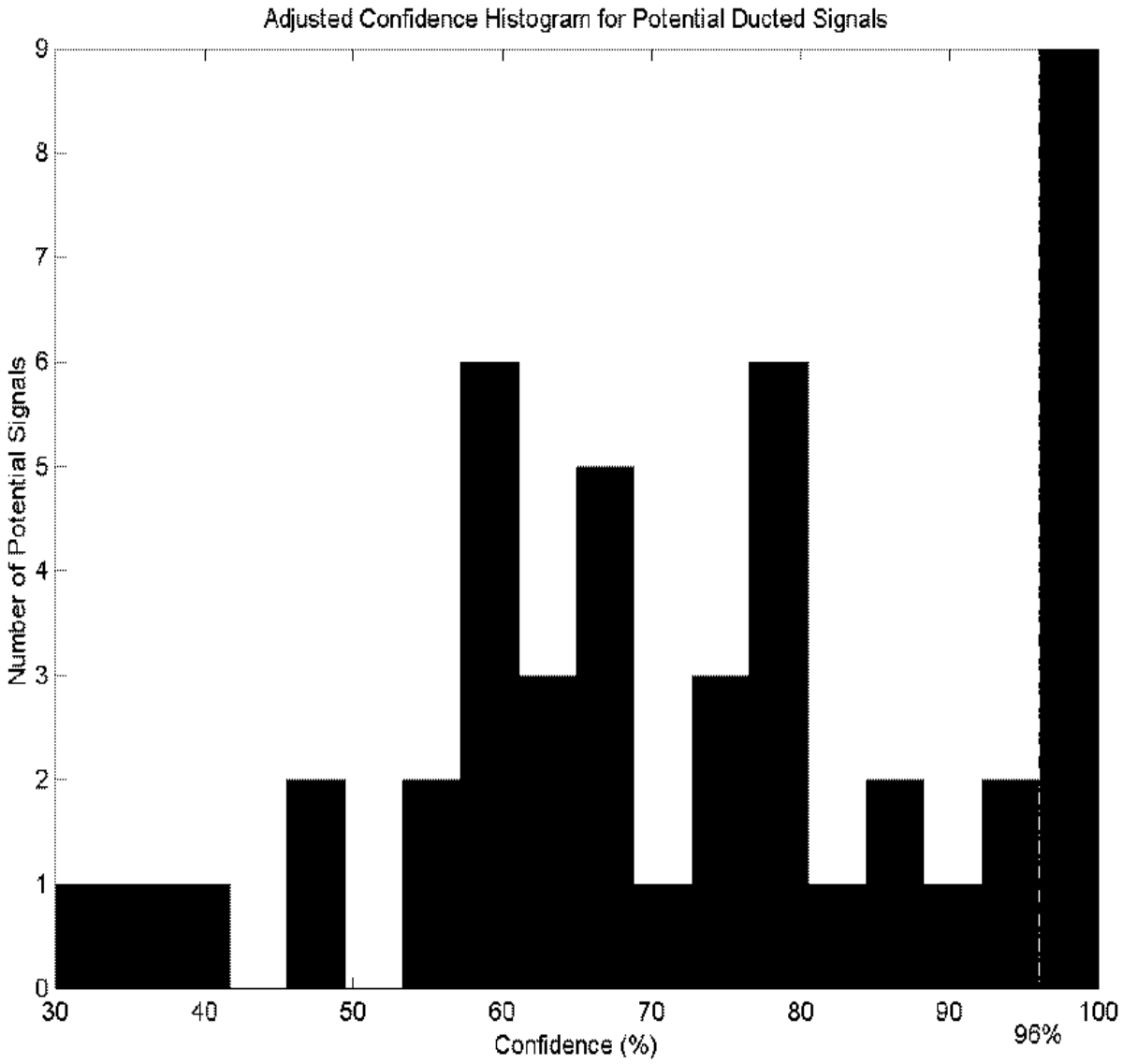
Adjusted Confidence Histogram for Potential Ducted Signals
Number of Potential Signals
Confidence (%)
96%
0
1
2
3
4
5
6
7
8
9
30
40
50
60
70
80
90
100